Journal of Applied Mechanics and Technical Physics, Vol. 45, No. 3, pp. 389–400, 2004

VISCOUS FILM FLOW DOWN CORRUGATED SURFACES

Yu. Ya. Trifonov

UDC 532.51

A theoretical analysis of a downward viscous film flow on corrugated surfaces is reported. The study is based on Navier–Stokes equations (for one- and two-dimensional surfaces) and on an integral model (for a three-dimensional surface with double corrugation). The calculations were carried out in a wide range of Reynolds numbers and geometric characteristics of the surface with due allowance for the surface-tension force. The shape of the free surface of the liquid film and other characteristics of the flow are calculated. It is shown that, in the case of a one-dimensional surface, there exists a range of parameters where the flow is predominantly governed by surface-tension forces; this flow can be adequately treated with the integral approach. In this range of parameters, on the surface with double corrugation, the average quantities of the downward flow in wide corrugation valleys are determined by the fine-texture geometry.

Key words: *viscous film flow, corrugated surfaces.*

1. INTRODUCTION AND FORMULATION OF THE PROBLEM

Theoretical studies of film flows date back to the pioneering work of Nusselt [1], in which an exact solution of Navier–Stokes equations for a free viscous thin-film flow down a smooth vertical wall was reported:

$$U_0(y) = \frac{3\nu\,\mathrm{Re}}{H_0}\Big(\frac{y}{H_0} - \frac{y^2}{2H_0^2}\Big), \qquad H_0 = \Big(\frac{3\nu^2\,\mathrm{Re}}{g}\Big)^{1/3}.$$

Here $U_0(y)$ is the film-flow velocity profile in the direction of the gravity force g, ν is the kinematic viscosity, and H_0 is the thickness of the liquid film for a given mass-flux density $\nu\,\mathrm{Re}$ of the liquid (Re is the Reynolds number).

Subsequent theoretical and experimental studies showed that the Nusselt solution is almost never encountered in practice: as a rule, waves are observed on the film surface. A great number of studies involved linear and nonlinear analyses of the wave-formation process [2–5]. The problem of nonlinear waves on a film falling down a smooth plate has much in common with the problem os a viscous flow over a corrugated surface. In both cases, the equations are essentially nonlinear, the shape of the free surface is not known beforehand, the surface-tension forces play an important part, and there is a spatial period involved in the problem.

In spite of the numerous applications of the problem under study to distillation processes [6, 7] and advanced heat exchangers [8, 9], the experimental [10, 11] and theoretical [12–19] studies of the film flow on a corrugated surface are few in number. For instance, the flow down a sine-shaped surface with a corrugation amplitude small compared to the Nusselt thickness of the liquid film was examined with the perturbation technique by Wang [12]. Kang and Chen [13] extended this approach to the case of a two-layer film flow along a corrugated surface with a small corrugation amplitude. Pozrikidis [14] considered a creep flow down a curved inclined surface, using the boundary-element method and disregarding inertial forces. The asymptotic approach was used by Shetty and Cerro [15] to examine a liquid flow down a corrugated surface with a corrugation amplitude much greater than the Nusselt film thickness. Treating corrugation in the linear approximation, Bontozoglou and Papapolymerou [16]

Kutateladze Institute of Thermophysics, Siberian Division, Russian Academy of Sciences, Novosibirsk 630090.
Translated from Prikladnaya Mekhanika i Tekhnicheskaya Fizika, Vol. 45, No. 3, pp. 97–110, May–June, 2004. Original article submitted March 31, 2003; revision submitted June 30, 2003.

0021-8944/04/4503-0389

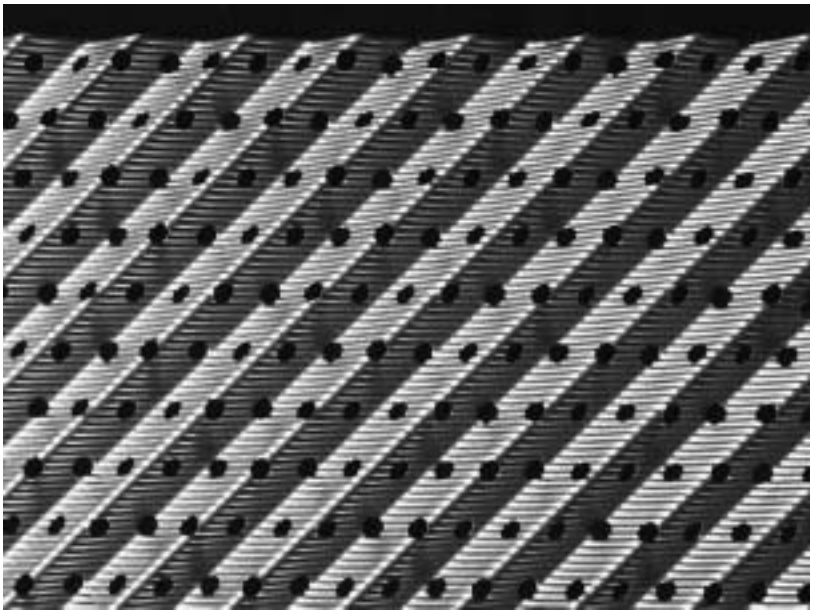

Fig. 1. Corrugated surface with rough corrugation and fine horizontal texture.

examined resonant effects in the range of finite Reynolds numbers. The numerical solution of the Navier–Stokes equation has allowed the present author [17, 18] to examine the film flow in the range of finite Reynolds numbers for corrugation amplitudes commensurable with the Nusselt thickness. In addition, in [17, 18], an integral approach was developed, and stability of the flow to free-surface disturbances was examined. In [19], the present author examined heat and mass transfer in a film flow down a corrugated surface. In all works mentioned above, the flow down a one-dimensional curved surface (corrugation along the flow direction) was considered. The main purpose of the present study was to examine the film flow on complicated three-dimensional surfaces (Fig. 1) with rough corrugation (with an amplitude much greater than the Nusselt thickness) and fine texture (with an amplitude commensurable with the Nusselt thickness).

2. GOVERNING EQUATIONS

2.1. One-Dimensional Corrugation. The film flow down a one-dimensional surface is described by a set of Navier–Stokes equations with appropriate boundary conditions [17]:

$$u\frac{\partial u}{\partial x}+v\frac{\partial u}{\partial y}=-\frac{1}{\rho}\frac{\partial P}{\partial x}+g+\nu\Big(\frac{\partial^2 u}{\partial x^2}+\frac{\partial^2 u}{\partial y^2}\Big),\qquad u\frac{\partial v}{\partial x}+v\frac{\partial v}{\partial y}=-\frac{1}{\rho}\frac{\partial P}{\partial y}+\nu\Big(\frac{\partial^2 v}{\partial x^2}+\frac{\partial^2 v}{\partial y^2}\Big),$$

$$\frac{\partial u}{\partial x}+\frac{\partial v}{\partial y}=0,\qquad u=v=0,\quad y=f(x),$$

$$\sigma_{ik}n_k n_i=-P_a+\frac{\sigma}{[1+(dh/dx)^2]^{3/2}}\frac{d^2h}{dx^2},\quad \sigma_{ik}n_k\tau_i=0,\quad i,k=1,2,\quad y=h(x),$$

$$v=u\frac{dh}{dx},\quad y=h(x),$$

$$\boldsymbol{n}=\frac{(-dh/dx,1)}{\sqrt{1+(dh/dx)^2}},\qquad \tau=\frac{(1,dh/dx)}{\sqrt{1+(dh/dx)^2}},\qquad \boldsymbol{u}=(u,v),\qquad \boldsymbol{x}=(x,y),$$

$$\sigma_{ik}=-P\delta_{ik}+\mu\Big(\frac{\partial u_i}{\partial x_k}+\frac{\partial u_k}{\partial x_i}\Big).$$

Here, u and v are the velocity components along the x and y axes, respectively, P is the pressure in the liquid, P_a is atmospheric pressure, ν and μ are the kinematic and dynamic viscosities, respectively, ρ is the density of the liquid, σ is the surface tension, $f(x)$ is the shape function of the corrugated wall, $h(x)$ is the shape function of the free surface of the liquid film, $H(x) = h(x) - f(x)$ is the local thickness of the liquid film, σ_{ik} are the stress-tensor components in the liquid, and n_k and τ_i are the normal and tangential unit vectors, respectively.

We use the transformation of coordinates $x = x$ and $\eta = (y - f(x))/H(x)$ (the flow region in the new variables becomes known: $x \in [0, L]$, $\eta \in [0, 1]$). Non-dimensionalizing the starting equations and combining the boundary conditions, we obtain the following set of equations for numerical calculations:

$$-\frac{\partial P_*}{\partial x_*} - \eta_x \frac{\partial P_*}{\partial \eta} + \frac{1}{\varepsilon \operatorname{Re}}\Big[3 + \eta_y^2 \frac{\partial^2 u_*}{\partial \eta^2} + \varepsilon^2\Big(\frac{\partial^2 u_*}{\partial x_*^2} + \eta_x^2 \frac{\partial^2 u_*}{\partial \eta^2} + 2\eta_x \frac{\partial^2 u_*}{\partial x\, \partial \eta}$$

$$+ (\eta_{x\xi} + \eta_x \eta_{x\eta}) \frac{\partial u_*}{\partial \eta}\Big)\Big] - \eta_y \frac{\partial u_* v_*}{\partial \eta} - \frac{\partial u_*^2}{\partial x_*} - \eta_x \frac{\partial u_*^2}{\partial \eta} = 0; \tag{2.1}$$

$$\frac{\partial (P_* - (P_a)_*)}{\partial \eta} = \frac{\varepsilon}{\operatorname{Re}}\Big[\eta_y^2 \frac{\partial^2 v_*}{\partial \eta^2} + \varepsilon^2\Big(\frac{\partial^2 v_*}{\partial x_*^2} + \eta_x^2 \frac{\partial^2 v_*}{\partial \eta^2} + 2\eta_x \frac{\partial^2 v_*}{\partial x_* \partial \eta}$$

$$+ (\eta_{x\xi} + \eta_x \eta_{x\eta}) \frac{\partial v_*}{\partial \eta}\Big)\Big] H_*(x_*) - \varepsilon^2\Big(H_* \frac{\partial u_* v_*}{\partial x_*} + H_* \eta_x \frac{\partial u_* v_*}{\partial \eta} + \frac{\partial v_*^2}{\partial \eta}\Big); \tag{2.2}$$

$$v_*(x_*, \eta) = -H_*(x_*) u_*(x_*, \eta) \eta_x - \frac{\partial}{\partial x_*}\Big(H_* \int_0^\eta u_*(x_*, \eta')\, d\eta'\Big); \tag{2.3}$$

$$H_*(x_*) \int_0^1 u_*(x_*, \eta')\, d\eta' = 1; \tag{2.4}$$

$$u_*(x_*, \eta) = 0, \qquad \eta = 0; \tag{2.5}$$

$$P_* - (P_a)_* = \frac{2\varepsilon}{\operatorname{Re}} \frac{1}{H_*(x_*)} \frac{\partial v_*}{\partial \eta}\Big[1 + \varepsilon^2\Big(\frac{d^2 H_*}{dx_*^2} + \frac{1}{\varepsilon_1}\frac{d^2 f_*}{dx_*^2}\Big)^2\Big] \Big/ \Big[1 - \varepsilon^2\Big(\frac{d^2 H_*}{dx_*^2} + \frac{1}{\varepsilon_1}\frac{d^2 f_*}{dx_*^2}\Big)^2\Big]$$

$$- \varepsilon^2 \operatorname{We}\Big(\frac{d^2 H_*}{dx_*^2} + \frac{1}{\varepsilon_1}\frac{d^2 f_*}{dx_*^2}\Big) \Big/ \Big[1 + \varepsilon^2\Big(\frac{dH_*}{dx_*} + \frac{1}{\varepsilon_1}\frac{df_*}{dx_*}\Big)^2\Big]^{3/2}, \quad \eta = 1; \tag{2.6}$$

$$\Big[\frac{\partial u_*}{\partial \eta} + \varepsilon^2 H_* \frac{\partial v_*}{\partial x_*} - \varepsilon^2\Big(\frac{dH_*}{dx_*} + \frac{1}{\varepsilon_1}\frac{df_*}{dx_*}\Big)\frac{\partial v_*}{\partial \eta}\Big]\Big[1 - \varepsilon^2\Big(\frac{dH_*}{dx_*} + \frac{1}{\varepsilon_1}\frac{df_*}{dx_*}\Big)^2\Big] + 4\varepsilon^2 \frac{\partial v_*}{\partial \eta}\Big(\frac{dH_*}{dx_*} + \frac{1}{\varepsilon_1}\frac{df_*}{dx_*}\Big) = 0, \quad \eta = 1. \tag{2.7}$$

Here $x_* = x/L$, $y_* = y/H_0$, $f_*(x) = f(x)/A$, $u_* = u/u_0$, $v_* = v/(\varepsilon u_0)$, $H_*(x) = H(x)/H_0$, $P_* = P/(\rho u_0^2)$, A is the corrugation amplitude, $u_0 = Q_0/H_0$, $\varepsilon = H_0/L$, $\varepsilon_1 = H_0/A$, H_0 is the Nusselt film thickness, $\operatorname{We} = (3\operatorname{Fi})^{1/3}/\operatorname{Re}^{5/3}$ is the Weber number, $\operatorname{Fi} = (\sigma/\rho)^3/(g\nu^4)$ is the film number, $\eta = (y - f(x)/\varepsilon_1)/H(x)$, $\eta_x = -[\eta\, dH/dx + (1/\varepsilon_1)\, df/dx]/H(x)$, $\eta_y = 1/H(x)$, $\eta_{x\eta} = -(1/H)\, dH/dx$, $\eta_{x\xi} = -(\eta_x/H)\, dH/dx - [\eta\, d^2H/dx^2 + (1/\varepsilon_1)\, d^2 f/dx^2]/H(x)$, and $Q_0 = \nu \operatorname{Re}$ is the mass-flux density of the liquid. In what follows, we omit the non-dimensionalization sign.

It follows from (2.1)–(2.7) that the flow of interest is governed by the following four independent parameters: Fi, $(\nu^2/g)^{1/3}/L$, A/L, and Re. The corrugation shape function $f(x)$ is also an independent variable. The problem is to find the unknown fields $u(x, y)$, $v(x, y)$, $P(x, y)$, and $H(x)$ for specified parameters. Equations (2.1)–(2.7) were solved numerically by the spectral method:

$$u(x, \eta) = \frac{1}{2} U_1(x) + \sum_{m=2}^{M} U_m(x) T_{m-1}(\eta_1), \qquad \eta_1 = 2\eta - 1,$$

$$U_m(x) = U_m^0 + \sum_{n=-N/2+1,\, n\neq 0}^{N/2-1} U_m^n \exp(2\pi i n x), \qquad (U_m^{-n})^* = U_m^n, \qquad m = 1, \ldots, M. \tag{2.8}$$

Here $T_m(\eta_1)$ are the Chebyshev polynomials; the asterisk denotes complex conjugation.

With known $M(N-1)$ values of harmonics U_m^n, the film thickness $H(x)$ can be uniquely reconstructed from Eq. (2.4), the velocity $v(x,\eta)$ from Eq. (2.3), and the pressure $P(x,\eta)$ from Eqs. (2.2) and (2.6). The numerical algorithm starts from a first-order approximation for U_m^n (e.g., from the Nusselt solution); this approximation is to be subsequently refined by the Newton method employing Eq. (2.1) in the (n,m)-space. The Jacobian matrix is calculated by a finite-difference scheme. The basis functions (2.8) do not automatically satisfy the boundary conditions (2.5) and (2.7). As a consequence, we have $(M+2)(N-1)$ nonlinear algebraic equations for $M(N-1)$ unknown quantities, i. e., an overdetermined system. In the present work, we omit $2(N-1)$ equations for the two last Chebyshev polynomials, small in value, in the decomposition of (2.1); instead, we use the boundary conditions (2.5) and (2.7). In test computations, other strategies for reducing the total number of equations were checked. With a good approximation for the function $u(x,\eta)$, the results are practically coincident. To approximate the function $u(x,\eta)$, the numbers N and M were varied so that the condition $|U_m^{N/2-1}|/\sup|U_m^n| < 10^{-3}$ for all m and the condition $|U_M^n|/\sup|U_m^n| < 10^{-3}$ for all n were always satisfied. A small difference between the solutions for different N and M (with an accurately fitted velocity field) additionally justifies the numerical procedure.

In examining the wave dynamics on the surface of liquid films flowing down a smooth surface, an integral approach (set of Shkadov's equations [20]) is frequently used. Here, long-wave disturbances are considered. In the case under study, similar equations can be obtained if one restricts consideration to the case of a corrugation wavelength far exceeding the film thickness ($\varepsilon \ll 1$). Note, for the majority of corrugated structures in use [6–9], this approximation is valid for fine corrugations. Below, the integral approach is used to calculate the flow down a surface with double corrugation. The main idea behind the integral approach consists in using a self-similar profile of streamwise velocity

$$u(x,y) = \frac{3\nu\,\mathrm{Re}}{H(x)}\Big(\frac{y-f(x)}{H(x)} - \frac{(y-f(x))^2}{2H^2}\Big). \tag{2.9}$$

This profile satisfies the boundary conditions with $\varepsilon \ll 1$ and Eq. (2.4). We substitute (2.9) into (2.1)–(2.7), omit small terms, and integrate across the film; then, we obtain the following set of equations governing the film-flow dynamics on the corrugated surface:

$$\frac{\partial q}{\partial t} + \frac{6}{5}\,\frac{\partial}{\partial x}\,\frac{q^2}{H} = \frac{3}{\varepsilon\,\mathrm{Re}}\Big(H - \frac{q}{H^2}\Big) + \varepsilon^2\,\mathrm{We}\,H\Big(\frac{\partial^3 H}{\partial x^3} + \frac{1}{\varepsilon_1}\,\frac{d^3 f}{dx^3}\Big),$$
$$\frac{\partial H}{\partial t} + \frac{\partial q}{\partial x} = 0. \tag{2.10}$$

Unsteady terms are added to provide for the most complete description of processes possible in the system. Note that the capillary term in (2.10) should be retained because the film number Fi in the Weber criterion is large for the majority of liquids.

In the present study, of interest are the following stationary solutions of (2.10): $H = H(x)$ and $q = 1$. Here, we have three independent parameters ($\varepsilon\,\mathrm{Re}$, $\varepsilon^2\,\mathrm{We}$, and ε_1), in contrast to Eqs. (2.1)–(2.7), which involve four parameters, Eq. (2.10) was solved numerically by the Newton method and Fourier expansion:

$$H(x) = \sum_{n=-N/2+1}^{N/2-1} H_n \exp(2\pi i n x), \qquad (H_{-n})^* = H_n.$$

In derivation of (2.10), we assumed that $\varepsilon_1 \approx 1$ (the corrugation amplitude and the film thickness are commensurable). In the case of rough corrugation, we have $\varepsilon_1 \ll 1$, and the integral approach yields the equation

$$\frac{6}{5}\,\frac{d}{ds}\Big(\frac{1}{H}\Big) = \frac{3}{\mathrm{Re}}\,\frac{d}{ds}\,(H^2\sin\theta) + \frac{3}{\varepsilon\,\mathrm{Re}}\Big(H\cos\theta - \frac{1}{H^2}\Big) + \varepsilon^2\,\mathrm{We}\,H\,\frac{d^3 H}{ds^3},$$
$$\cos\theta = \frac{1}{\sqrt{1+((\varepsilon/\varepsilon_1)\,df/dx)^2}}\Big|_{x=x(s)}, \qquad \sin\theta = \frac{(\varepsilon/\varepsilon_1)\,df/dx}{\sqrt{1+((\varepsilon/\varepsilon_1)\,df/dx)^2}}\Big|_{x=x(s)}, \tag{2.11}$$
$$s = \int_0^x \sqrt{1+\Big(\frac{\varepsilon}{\varepsilon_1}\,\frac{df}{dx}\Big)^2}\;dx_1.$$

Here, s is the "boundary-layer" variable; the film thickness is counted off in the direction normal to the solid surface. The periodic functions $\cos\theta(s)$ and $\sin\theta(s)$ are calculated from the corrugation shape.

2.2. Two-Dimensional Corrugation. In the case of oblique corrugation (α is the anticlockwise counted angle of inclination of the corrugation to the horizon and the coordinate z is directed along the corrugation), the equations of motion in the (x, y) plane and in the z direction can be split if the mass flux of the liquid is set across the corrugation. In a dimensionless form, Eqs. (2.1)–(2.11) remain unchanged, and the force g should be replaced by $g\cos\alpha$ in all dimensionless complexes. Note that the Reynolds number here is based on the mass-flux density across the rib: $\mathrm{Re} = \mathrm{Re}_{\mathrm{across}}$.

With the fields of u, v, P, and H found from Eqs. (2.1)–(2.7), the field of the velocity w in the z direction can be found from the following equations:

$$-\eta_y\frac{\partial wv}{\partial\eta} - \frac{\partial wu}{\partial x} - \eta_x\frac{\partial wu}{\partial\eta} + \frac{1}{\varepsilon\,\mathrm{Re}}\Big[\eta_y^2\frac{\partial^2 w}{\partial\eta^2} + \varepsilon^2\Big(\frac{\partial^2 w}{\partial x^2} + \eta_x^2\frac{\partial^2 w}{\partial\eta^2} + 2\eta_x\frac{\partial^2 w}{\partial x\,\partial\eta}$$

$$+ (\eta_{x\xi} + \eta_x\eta_{x\eta})\frac{\partial u}{\partial\eta}\Big)\Big] = -\frac{3}{\varepsilon\,\mathrm{Re}}\tan\alpha, \qquad Q(x) = H\int\limits_0^1 w(x,\eta)\,d\eta, \tag{2.12}$$

$$\frac{1}{H}\frac{\partial w}{\partial\eta}\Big[1 + \varepsilon^2\Big(\frac{dH}{dx} + \frac{1}{\varepsilon_1}\frac{df}{dx}\Big)^2\Big] - \varepsilon^2\frac{\partial w}{\partial x}\Big(\frac{dH}{dx} + \frac{1}{\varepsilon_1}\frac{df}{dx}\Big) = 0, \qquad \eta = 1,$$

$$w(x,\eta) = 0, \qquad \eta = 0.$$

For long-wave corrugation and an amplitude commensurable with the film thickness, Eq. (2.10) should be supplemented by the following equation for the flow rate Q along the rib:

$$\frac{6}{5}\frac{d}{dx}\Big(\frac{Q}{H}\Big) = \frac{3}{\varepsilon\,\mathrm{Re}}\Big(H\tan\alpha - \frac{Q}{H^2}\Big). \tag{2.13}$$

In the case of rough corrugation ($\varepsilon_1 \ll 1$), the equation that supplements (2.11) coincides with (2.13) with x replaced by s.

In all the three cases (Navier–Stokes equation, $\varepsilon \ll 1$, and $\varepsilon_1 \ll 1$), the mass-flux density in the vertical direction can be calculated by the formula

$$\mathrm{Re}_{\mathrm{vert}} = \mathrm{Re}\cos\alpha(1 + \langle Q\rangle\tan\alpha), \tag{2.14}$$

where the broken brackets denote the mean value along the x or s coordinate.

Note, if the film flow is directed across the ribs, the problem of finding the shape of the free surface of the liquid film and the velocity and pressure fields has a solution throughout the whole range of Reynolds numbers and inclination angles α, and for an arbitrary geometry of the rib. As is shown below, if the film flow is directed along the gravity force [Eq. (2.14) is solved simultaneously with the equations of motion], there may exist ranges of parameters where no solution with a completely wetted surface exists.

2.3. Three-Dimensional Surface with Rough Corrugation and Fine Texture. We consider the flow down a plate with a large corrugation period L in the x direction and fine texture with a period L_s. The z coordinate is directed along the rough-corrugation axis, and the resultant surface profile is

$$F_{3d}(x,z) = AF(x/L) + A_s f((x\cos\varphi - z\sin\varphi)/L_s). \tag{2.15}$$

Here, $F(x)$ is the dimensionless profile of rough corrugation, A is the rough-corrugation amplitude, α is the angle of inclination of rough corrugation to the horizon, L is the rough-corrugation period, $f(\xi)$ is the dimensionless profile of fine texture, A_s is the amplitude of the fine texture, α_s is the angle of inclination of fine texture to the horizon, L_s is the fine-texture period, and $\varphi = \alpha_s - \alpha$ is the angle of inclination of fine texture to the rough-corrugation axis. Note that the function $F_{3d}(x,z)$ is not periodic in the x and z directions. For this reason, an oblique transformation of coordinates is used below.

The viscous film flow down the surface under consideration is a complex three-dimensional problem. Here, the Navier–Stokes calculation of the free surface and the velocity field involves considerable computational difficulties. As is shown in [17, 18] and in the present work, there exists a range of Reynolds numbers in which the flow along the plate with one- or two-dimensional corrugation can be adequately described by the integral model. Therefore, it becomes possible to develop the integral approach for the film flow down a plate with profile (2.15).

Next, we use the "boundary-layer" coordinate s directed along the solid surface formed by rough corrugation and the local coordinate y normal to this surface. We restrict ourselves to the case in which the spatial period of fine texture is much greater than the film thickness. The simplified equations have the following form:

$$u\,\frac{\partial u}{\partial s}+v\,\frac{\partial u}{\partial y}+w\,\frac{\partial u}{\partial z}=-\frac{1}{\rho}\,\frac{\partial P}{\partial s}+g\cos\alpha\cos\theta+\nu\,\frac{\partial^2 u}{\partial y^2},$$

$$-\frac{1}{\rho}\,\frac{\partial P}{\partial y}-g\cos\alpha\sin\theta=0,$$

$$u\,\frac{\partial w}{\partial s}+v\,\frac{\partial w}{\partial y}+w\,\frac{\partial w}{\partial z}=-\frac{1}{\rho}\,\frac{\partial P}{\partial z}+g\sin\alpha+\nu\,\frac{\partial^2 u}{\partial y^2},$$

$$\frac{\partial u}{\partial s}+\frac{\partial v}{\partial y}+\frac{\partial w}{\partial z}=0,$$

$$u=v=w=0,\qquad y=A_s f(s,z),$$

$$P=P_a-\sigma\Big(\frac{\partial^2 h}{\partial s^2}+\frac{\partial^2 h}{\partial z^2}\Big),\qquad \frac{\partial u}{\partial y}=\frac{\partial w}{\partial y}=0,\qquad y=h(s,z),$$

$$v=u\,\frac{\partial h}{\partial s}+w\,\frac{\partial h}{\partial z},\qquad y=h(s,z),$$

$$h(s,z)=H(s,z)+A_s f(s,z),\qquad f(s,z)=f((s\cos\varphi-z\sin\varphi)/L_s),$$

$$\cos\theta=\frac{1}{\sqrt{1+(A\,dF/dx)^2}}\Big|_{x=x(s)},\qquad \sin\theta=\frac{A\,dF/dx}{\sqrt{1+(A\,dF/dx)^2}}\Big|_{x=x(s)},$$

$$s=\int\limits_0^x\sqrt{1+\Big(A\,\frac{dF}{dx_1}\Big)^2}\,dx_1.$$

Here, the functions $\cos\theta$ and $\sin\theta$ are determined by the rough-corrugation geometry.

Next, we use self-similar velocity profiles that satisfy the boundary conditions

$$u(y,s,z)=\frac{3q(s,z)}{H(s,z)}\Big[\frac{y-A_s f(s,z)}{H(s,z)}-\frac{1}{2}\Big(\frac{y-A_s f(s,z)}{H(s,z)}\Big)^2\Big],$$

$$w(y,s,z)=\frac{3Q(s,z)}{H(s,z)}\Big[\frac{y-A_s f(s,z)}{H(s,z)}-\frac{1}{2}\Big(\frac{y-A_s f(s,z)}{H(s,z)}\Big)^2\Big].$$

Integrating across the liquid film, we obtain

$$\frac{6}{5}\,\frac{\partial}{\partial s}\,\frac{q^2}{H}+\frac{6}{5}\,\frac{\partial}{\partial z}\,\frac{qQ}{H}=gH\cos\alpha\cos\theta-\frac{3\nu q}{H^2}-\frac{1}{\rho}\,H\,\frac{\partial P^*}{\partial s}$$

$$-g\cos\alpha\,\frac{\partial}{\partial s}\Big(\frac{H^2}{2}\,\sin\theta\Big)-gHA_s\,\frac{\partial f}{\partial s}\,\cos\alpha\sin\theta,$$

$$\frac{6}{5}\,\frac{\partial}{\partial z}\,\frac{Q^2}{H}+\frac{6}{5}\,\frac{\partial}{\partial s}\,\frac{qQ}{H}=gH\sin\alpha-\frac{3\nu Q}{H^2}-\frac{1}{\rho}\,H\,\frac{\partial P^*}{\partial z}$$

$$-g\cos\alpha\sin\theta\,\frac{\partial}{\partial z}\Big(\frac{H^2}{2}\Big)-gHA_s\,\frac{\partial f}{\partial z}\,\cos\alpha\sin\theta,$$

$$\frac{\partial Q}{\partial z}+\frac{\partial q}{\partial s}=0,\qquad P^*=-\sigma\Big(\frac{\partial^2 h}{\partial s^2}+\frac{\partial^2 h}{\partial z^2}\Big),\qquad h(s,z)=H(s,z)+A_s f(s,z).$$

Here, q is the local flow rate along the coordinate s (across large ribs) and Q is the flow rate in the z direction (along large ribs).

Next, we use the transformation of variables

$$s=s,\quad \xi=s\cos\varphi-z\sin\varphi,\quad \frac{\partial}{\partial s}\to\frac{\partial}{\partial s}+\cos\varphi\,\frac{\partial}{\partial\xi},\quad \frac{\partial}{\partial z}\to-\sin\varphi\,\frac{\partial}{\partial\xi}$$

and the following dimensional quantities: s/L_1, ξ/L_s and $l = L_s/L_1$ (L_1 is the perimeter of one period of each large rib), q/Q_0 and Q/Q_0 (Q_0 is the flow rate along the gravity force), and H/H_0 [$H_0 = (3\nu Q_0/(g\cos\alpha))^{1/3}$]. After some rearrangements, we have

$$\Big(l\,\frac{\partial}{\partial s} + \cos\varphi\,\frac{\partial}{\partial\xi}\Big)\Big(\frac{6}{5}\,\frac{q^2}{H} + \frac{1.5}{\mathrm{Re}}\,H^2\sin\theta\Big) - \sin\varphi\,\frac{\partial}{\partial\xi}\Big(\frac{6}{5}\,\frac{qQ}{H}\Big)$$

$$= \frac{3}{\varepsilon\,\mathrm{Re}}\Big(H\cos\theta - \frac{q}{H^2}\Big) - \varepsilon^2\,\mathrm{We}\,H\Big(l\,\frac{\partial}{\partial s} + \cos\varphi\,\frac{\partial}{\partial\xi}\Big)P^* - \frac{3\varepsilon_1}{\mathrm{Re}}\,H\sin\theta\cos\varphi\,\frac{df}{d\xi}; \tag{2.16}$$

$$\Big(l\,\frac{\partial}{\partial s} + \cos\varphi\,\frac{\partial}{\partial\xi}\Big)\Big(\frac{6}{5}\,\frac{qQ}{H}\Big) - \sin\varphi\,\frac{\partial}{\partial\xi}\Big(\frac{6}{5}\,\frac{Q^2}{H} + \frac{1.5}{\mathrm{Re}}\,H^2\sin\theta\Big)$$

$$= \frac{3}{\varepsilon\,\mathrm{Re}}\Big(H\tan\,\alpha - \frac{Q}{H^2}\Big) + \varepsilon^2\,\mathrm{We}\,H\sin\varphi\,\frac{\partial P^*}{\partial\xi} + \frac{3\varepsilon_1}{\mathrm{Re}}\,H\sin\theta\sin\varphi\,\frac{df}{d\xi}; \tag{2.17}$$

$$\Big(l\,\frac{\partial}{\partial s} + \cos\varphi\,\frac{\partial}{\partial\xi}\Big)q - \sin\varphi\,\frac{\partial Q}{\partial\xi} = 0, \quad P^* = -\Big(l^2\,\frac{\partial^2}{\partial s^2} + 2\cos\varphi\,\frac{\partial^2}{\partial s\,\partial\xi} + \frac{\partial^2}{\partial\xi^2}\Big)h(s,\xi); \tag{2.18}$$

$$\langle\langle Q\rangle\rangle\sin\alpha + \langle\langle q\rangle\rangle\cos\alpha = 1, \qquad h(s,\xi) = H(s,\xi) + f(\xi)/\varepsilon_1. \tag{2.19}$$

Here

$$\cos\theta = \frac{1}{\sqrt{1 + ((A/L)\,dF/dx)^2}}\Big|_{x=x(s)}, \qquad s = \frac{L}{L_1}\int\limits_0^x \sqrt{1 + \Big(\frac{A}{L}\,\frac{dF}{dx_1}\Big)^2}\,dx_1,$$

$\varepsilon = H_0/L_s$, $\varepsilon_1 = H_0/A_s$, $\mathrm{We} = (3\,\mathrm{Fi})^{1/3}/\,\mathrm{Re}^{5/3}$, and $\mathrm{Fi} = (\sigma/\rho)^3/(g\nu^4\cos\alpha)$. The double broken brackets denote averaging over the coordinates s and z.

In the problem under consideration, we have two shape functions for the rough- and fine-corrugation profiles, and eight independent dimensionless parameters: $(3\nu^2/g)^{1/3}/L_s$, $A_s/(3\nu^2/g)^{1/3}$, $(\sigma/\rho g)/L_s^2$, L_s/L_1, A/L, α, φ, and Re number. Equations (2.16)–(2.19) were solved numerically by the spectral method:

$$H(s,\xi) = \sum_{m=-M/2+1}^{M/2-1}\ \sum_{n=-N/2+1}^{N/2-1} H_{nm}\exp(2\pi i n s)\exp(2\pi i m\xi), \qquad (H_{-n,-m})^* = H_{n,m},$$

$$Q(s,\xi) = \sum_{m=-M/2+1}^{M/2-1}\ \sum_{n=-N/2+1}^{N/2-1} Q_{nm}\exp(2\pi i n s)\exp(2\pi i m\xi), \qquad (Q_{-n,-m})^* = Q_{n,m},$$

$$q(s,\xi) = \sum_{m=-M/2+1}^{M/2-1}\ \sum_{n=-N/2+1}^{N/2-1} q_{nm}\exp(2\pi i n s)\exp(2\pi i m\xi), \qquad (q_{-n,-m})^* = q_{n,m}.$$

It follows from (2.18) that

$$q_{nm} = \begin{cases} mQ_{nm}\sin\varphi/(nl + m\cos\varphi), & n \neq 0,\ m \neq 0,\ \varphi \neq \pi/2, \\ (1 - Q_{00}\sin\alpha)/\cos\alpha, & n = 0,\ m = 0. \end{cases}$$

Thus, the problem is reduced to finding the unknown harmonics H_{nm} and Q_{nm}; this problem can be numerically solved by the Newton method. The case of $\varphi = \pi/2$ is degenerate with the symmetry $Q_{0m} = 0$. In this case, the harmonics q_{0m} can be found from Eqs. (2.16) and (2.17).

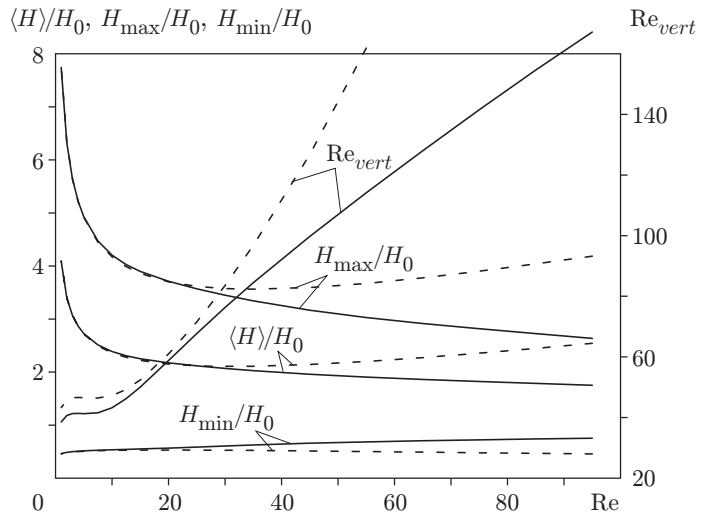

Fig. 2. Two-dimensional corrugation with $\alpha = 30°$: the solid and dashed curves show the calculations by the Navier–Stokes equation and integral model, respectively.

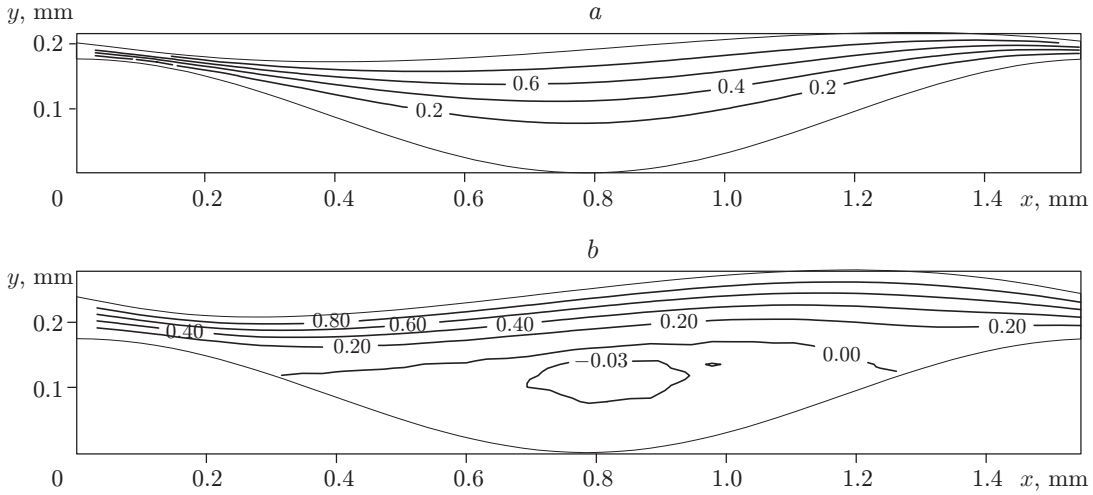

Fig. 3. Stream-function isolines for the corrugation angle $\alpha = 30°$ and Re = 5 (a) and 45 (b).

3. CALCULATION RESULTS

3.1. Two-Dimensional Corrugation. The data calculated by the Navier–Stokes equations (2.1)–(2.7), (2.12), (2.14) and by the integral model (2.10), (2.13), (2.14) are plotted in Figs. 2 and 3. We considered a corrugated surface with the following geometric parameters: $A = 0.175$ mm (commensurable with the Nusselt film thickness), $L = 1.57$ mm, and $f(x) = 0.5(1 - \cos(2\pi x))$. Note that these parameters are close to respective characteristics of fine texture for elements of the Sulzer 500Y industrial unit [6]. The computations were performed for a low-viscosity liquid (nitrogen at the saturation curve under atmospheric pressure) for $\alpha = 30°$. Figure 2 shows the main free-surface characteristics versus the Reynolds number. Figure 3 shows the isolines of the stream function Ψ ($u = \partial\Psi/\partial y$, $v = -\partial\Psi/\partial x$) for Re = 5 and 45.

The computations performed for the flow down a plate with oblique fine corrugation allows the following conclusions to be drawn.

For low Reynolds numbers, "thick" and thin flow regions are formed in the valleys and on the corrugation peaks, respectively. The film thickness is minimum on the slope of the solid surface in the vicinity of the peaks.

With increasing Reynolds number, the free surface becomes more straight and the texture is "flooded" by the liquid.

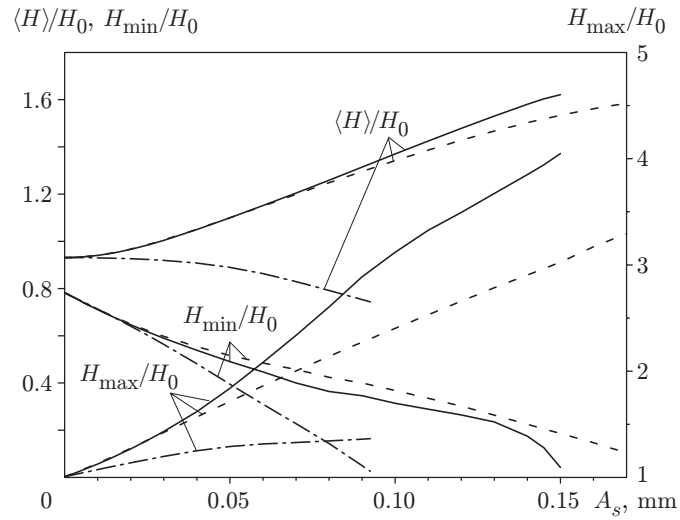

Fig. 4. Film thickness versus the fine-corrugation amplitude for the flow down a surface with double corrugation: solid curves refer to $\alpha_s = 8^\circ$ (almost horizontal texture), dashed curves refer to $\alpha_s = -27^\circ$ (oblique texture), and dot-and-dashed curves refer to $\alpha_s = -90^\circ$ (vertical texture).

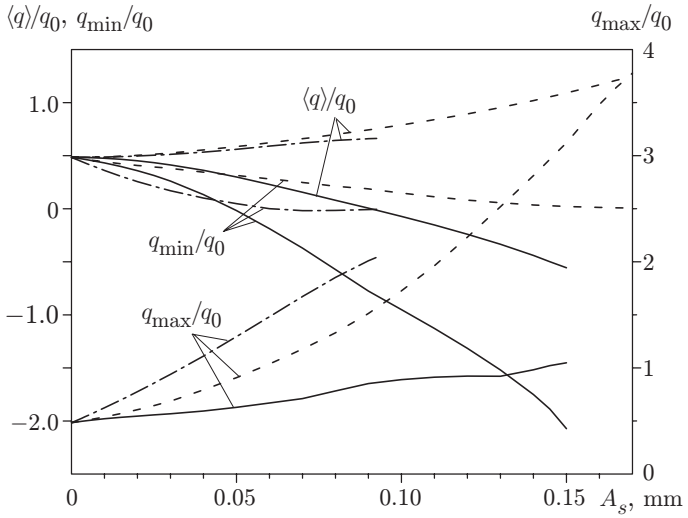

Fig. 5. Flow rate across large ribs versus the fine-texture amplitude for the flow down a surface with double corrugation: $\alpha_s = 8^\circ$ (solid curves), -27° (dashed curves), and -90° (dot-and-dashed curves).

In the examined range of Reynolds numbers, two regions can be distinguished. The flow is mainly determined by surface-tension forces in the region of low and moderate Reynolds numbers and by inertial forces in the region of high Reynolds numbers.

In the region where the flow is determined by surface-tension forces, the data calculated by the integral model are in good agreement with the data calculated by the Navier–Stokes equations. For the flow down a plate with rough corrugation, good agreement is observed between the values calculated by both models in a wide range of Reynolds numbers, corrugation angles, and corrugation parameters. In this case, the capillary and inertial terms are negligible, and the flow can be accurately predicted by the following formulas for the dimensionless film thickness and flow rates:

$$H(s) = (1/\cos\theta)^{1/3}, \quad q(s) = 1, \quad Q(s) = \tan\alpha/\cos\theta, \quad \mathrm{Re}_{\mathrm{vert}} = \mathrm{Re}\cos\alpha(1 + \langle Q\rangle\tan\alpha).$$

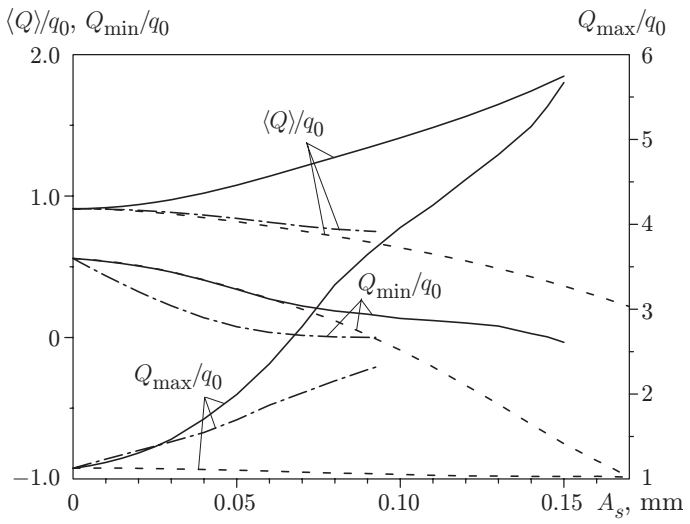

Fig. 6. Flow rate along large ribs versus the fine-texture amplitude for the flow down a surface with double corrugation: $\alpha_s = 8^\circ$ (solid curves), -27° (dashed curves), and -90° (dot-and-dashed curves).

3.2. Three-Dimensional Surface with Rough Corrugation and Fine Texture. Figures 4–7 show the calculation results for the flow down a plate with double corrugation. As in Sec. 3.1, the dimensionless shape of rough and fine corrugations was set cosine. The computations were performed for nitrogen at the saturation curve under atmospheric pressure. It follows from Eqs. (2.16)–(2.19) that the problem still involves many parameters even if the physical properties of the liquid are fixed. We restrict ourselves to the case of a certain particular geometry of large ribs ($A = 6.5$ mm, $L = 11$ mm, and $\alpha = 48^\circ$), one Reynolds number (Re = 30), and a fixed fine-corrugation period $L_s = 1.57$ mm. Note that the indicated values of geometric parameters are close to respective characteristics of individual elements of the Sulzer 500Y industrial unit [6] (Fig. 1). In Figs. 4–6, the fine-corrugation amplitude was varied from zero to a limiting value for which a solution with a completely wetted solid surface could be obtained. The angle of inclination of fine corrugation was also varied in the calculations. The chosen values of parameters are within the region where the data for one- and two-dimensional flows calculated by integral models are in good agreement with the data calculated by full Navier–Stokes equations.

Figures 4–6 shows three characteristics (film thickness H, flow rate q across large ribs, and flow rate Q along large ribs) versus the fine-corrugation amplitude, respectively.

Figure 7 shows the film-thickness distribution over one rough-corrugation period in the s and z directions for three angles of inclination of fine texture. The values of the fine-texture amplitude are close to the corresponding limiting values: $A_s = 0.15$ (a), 0.17 (b), and 0.0925 mm (c). Note that Fig. 7 rotated anticlockwise by 42° gives a picture corresponding to a physical plane with a downward directed force of gravity. Note also that the large corrugation rib has a peak at $x = 5.5$ mm.

The performed modeling of the flow down the plate with double corrugation allows the following conclusions to be drawn.

For all fine-texture inclination angles, there is a limiting texture amplitude below which there exists a solution with a completely wetted solid surface. For larger texture amplitudes, apparently, dry regions will emerge on the solid surface. In the latter case, the distributions of the film thickness and flow rates in the vicinity of the critical amplitude are more complicated. Apart from the regions where the film is thin, there are regions where the film thickness and the flow rate are quite substantial.

The angle of inclination of fine texture has a pronounced effect on average flow parameters. With increasing amplitude of horizontal texture, the mean flow rate along large ribs increases and the mean flow rate across large ribs decreases. The opposite tendency is displayed by vertical and oblique textures.

This work was supported by INTAS (Grant No. 99-1107) and by the Russian Foundation for National Science.

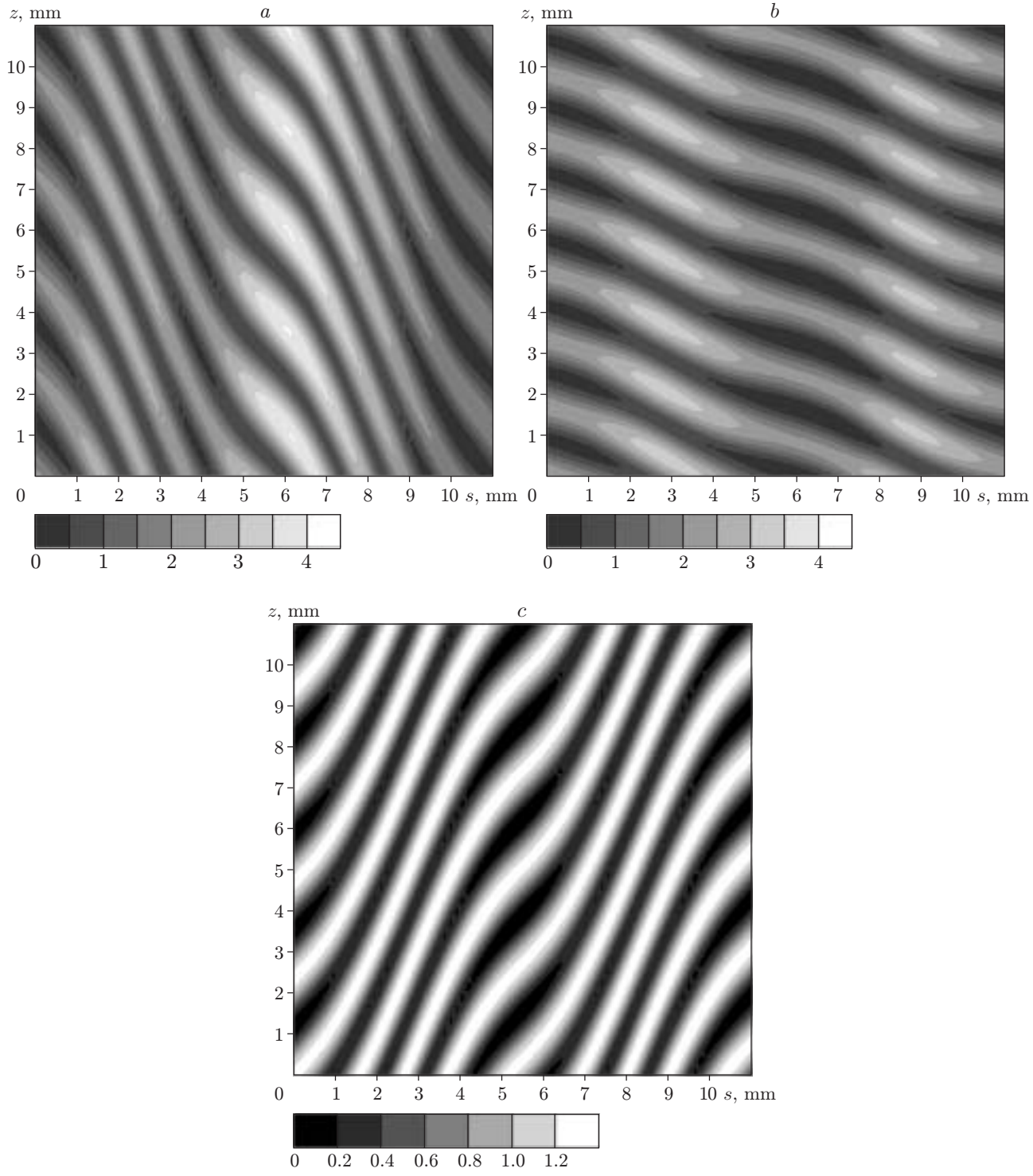

Fig. 7. Film-thickness distribution over one rough-corrugation period in the s and z directions: $\alpha_s = 8^\circ$ (almost horizontal texture) (a), $\alpha_s = -27^\circ$ (oblique texture) (b), and $\alpha_s = -90^\circ$ (vertical texture) (c).

REFERENCES

1. W. Nusselt, "Die Oberflächenkondensation des Wasserdampfes," *Zeitschrift VDI*, **60**, 541–546 (1916).
2. S. V. Alekseenko, V. E. Nakoryakov, and B. G. Pokusaev, *Wavy Liquid Film Flow* [in Russian], Nauka, Novosibirsk (1992).
3. H.-C. Chang, "Wave evolution on a falling film," *Ann. Rev. Fluid Mech.*, **26**, 103–136 (1994).
4. Yu. Ya. Trifonov and O. Yu. Tsvelodub, "Nonlinear waves on the surface of a falling liquid film. Pt 1. Waves of the first family and their stability," *J. Fluid Mech.*, **229**, 531–554 (1991).
5. L. T. Nguyen and V. Balakotaiah, "Modeling and experimental studies of wave evolution on free falling viscous films," *Phys. Fluids*, **12**, 2236–2256 (2000).
6. J. R. Fair and J. R. Bravo, "Distillation columns containing structure packing," *Chem. Eng. Progr.*, **86**, 19–29 (1990).
7. J. M. DeSantos, T. R. Melli, and L. E. Scriven, "Mechanics of gas-liquid flow in packed-bed contactors," *Ann. Rev. Fluid Mech.*, **23**, 233–260 (1991).
8. R. K. Shah and W. W. Focke, "Plate heat exchangers and their design theory," in: Heat transfer equipment design, Hemisphere, Washington (1988), pp. 227–254.
9. R. L. Webb, *Principles of Enhanced Heat Transfer*, Wiley, New York (1994).
10. L. Zhao and R. L. Cerro, "Experimental characterization of viscous film flows over complex surfaces," *Int. J. Multiphase Flow*, **6**, 495–516 (1992).
11. M. Vlachogiannis and V. Bontozoglou, "Experiments on laminar film flow along a periodic wall," *J. Fluid Mech.*, **457**, 133–156 (2002).
12. C. Y. Wang, "Liquid film flowing slowly down a wavy incline," *AIChE J.*, **27**, 207–212 (1981).
13. F. Kang and K. Chen, "Gravity-driven two-layer flow down a slightly wavy periodic incline at low Reynolds numbers," *Int. J. Multiphase Flow*, **3**, 501–513 (1995).
14. C. Pozrikidis, "The flow of a liquid film along a periodic wall," *J. Fluid Mech.*, **188**, 275–300 (1988).
15. S. Shetty and R. L. Cerro, "Flow of a thin film over a periodic surface," *Int. J. Multiphase Flow*, **6**, 1013–1027 (1993).
16. V. Bontozoglou and G. Papapolymerou, "Laminar film flow down a wavy incline," *Int. J. Multiphase Flow*, **1**, 69–79 (1997).
17. Yu. Ya. Trifonov, "Viscous liquid film flows over a periodic surface," *Int. J. Multiphase Flow*, **24**, 1139–1161 (1998).
18. Yu. Ya. Trifonov, "Viscous liquid film flows over a vertical corrugated surface and the film free surface stability," *Russ. J. Eng. Thermophys.*, **10**, No. 2, 129–145 (2000).
19. Yu. Ya. Trifonov, "Viscous liquid film flows over a vertical corrugated surface. Calculation of heat and mass transfer," in: Advanced computational methods in heat transfer VI. WITpress, Southhampton, UK (2000), pp. 373–382.
20. V. Ya. Shkadov, "Wavy modes of gravity-driven viscous thin-film flow," *Izv. Akad. Nauk SSSR, Mekh. Zhidk. Gaza*, **1**, 43–51 (1967).